PROGRESS IN COLOR, COLORANTS AND COATINGS

available online @ www.pccc.icrc.ac.ir

Progress in Color Colorants Coating 19 (2026), 47-65

Ministry of Science, Research and Technology
Institute for Color Science & Technology

Investigating the Effect of Zinc Oxide Nanoparticles on the Absorption of Ultraviolet Radiation for Enhancing the Efficacy of Sunscreen Products

M. Gozalabad Ghorbani[1, 2], A. Ghazitabar[*3], F. Gholami[1,2], M. Naderi[1,2], D. Fatmehsari Haghshenas[1,2]

[1.] Department of Material and Metallurgical Engineering, Amirkabir University of Technology, P.O. Box 15875-4413, Tehran, Iran.

[2.] Graphene and Advanced Materials Laboratory (GAMLab.), Amirkabir University of Technology, P.O. Box 15875-4413, Tehran, Iran

[3.] Department of Inorganic Pigments and Glazes, Institute for Color Science and Technology, P. O. Box: 16765-654, Tehran, Iran.

ARTICLE INFO

Article history:
Received: 22 Feb 2025
Final Revised: 04 May 2025
Accepted: 07 May 2025
Available online: 23 Sep 2025

Keywords:
Morphology
Sunscreen cream
Sun protection factor
UV radiation
ZnO

ABSTRACT

The degradation of the ozone layer and the consequent increase in ultraviolet (UV) radiation exposure have heightened interest in the development of mineral-based sunscreens. This study investigates the absorption characteristics of ultraviolet waves in mineral-based sunscreens formulated with various nanostructures of Zinc Oxide (ZnO), characterized by differing sizes (ranging from 40 to 70 nm) and morphologies, including plate-like, spherical, hedgehog-shaped, and irregular forms (predominantly rods). The protective efficacy against ultraviolet radiation was assessed using a visible-ultraviolet spectrometer and a diffuse reflectance spectrometer. The results indicate that most morphologies and dimensions of ZnO nanoparticles enhance the surface area available for the reflection and scattering of ultraviolet rays, thereby increasing the level of protection. Notably, the Z1 sample, exhibiting the plate-like morphology with a plate size of 71 nm, demonstrated the highest absorption rate. Additionally, the study reveals that increasing the concentration of ZnO in sunscreen formulations up to a critical threshold of 15 wt. % enhances UV protection; however, further increases to 21 wt. % result in a decline in protective efficacy. The sun protection factor (SPF) for the Z1 sample, which exhibited the highest level of protection, was calculated to be 47, indicating its potential suitability for commercialization in mineral-based sunscreen products. Prog. Color Colorants Coat. 19 (2026), 47-65© Institute for Color Science and Technology.

1. Introduction

In recent years, there has been a notable increase in public awareness regarding the detrimental effects of ultraviolet (UV) rays of the sun on the skin, which include premature aging and an elevated risk of skin cancer [1, 2]. Consequently, there has been a significant rise in interest in the use of skin protection products designed to shield against UV radiation [3]. Ultraviolet (UV) radiation is classified into three primary categories based on electrophysical properties and wavelength: UV-A (315-400 nm), UV-B (280-315 nm), and UV-C (100-280 nm) [4]. Each category has distinct characteristics and biological implications that can influence human health. Various strategies can be employed to protect the skin against UV rays, including natural compounds, protective clothing [5], and dietary antioxidants. The regular application of sunscreens, as a protective cosmetic product, can enhance the resistance

*Corresponding author: * Ghazitabar-a@icrc.ac.ir
https://doi.org/10.30509/PCCC.2025.167471.1365

of the skin against exogenous oxidative stress occurring in daily life, besides having the advantages of photoprotection [3, 4, 6].

Physical sunscreens offer several advantages over their chemical counterparts, including enhanced stability against sunlight, longer lasting, and, most notably, reduced skin sensitivity. Chemical sunscreens function by absorbing certain UV rays, subsequently emitting a portion of that energy at a lower intensity while dissipating some energy as heat [7]. In contrast, physical sunscreens operate through mechanisms of absorption, reflection, scattering, and energy conversion [8]. Ideally, sunscreens should exhibit minimal skin penetration, provide high levels of protection, demonstrate acceptable light fastness, and maintain visibility with minimal residue [9]. Considering the growing concerns about chemical sunscreens and the inclination to use more natural compounds, researchers have consistently endeavored to incorporate pure minerals such as Zinc Oxide (ZnO) [10], Titanium Dioxide (TiO_2) [11, 12], Magnesium Sulfate ($MgSO_4$) [13], and Iron Oxides [14] in sunscreen formulations for higher efficiency. In the development of UV protection methods, varying concentrations of materials, particularly titanium dioxide and ZnO, have been employed as UV radiation absorbents [15, 16]. These formulations contribute to maintaining skin health and attract attention for their aesthetic benefits [17].

Titanium dioxide, characterized by a higher refractive index compared to ZnO, tends to impart a whiter appearance to the skin, which may deter individuals from its use. To reduce this whitening effect, two strategies have been proposed: the incorporation of approved pigments and the utilization of nanoparticles [16, 18, 19]. While titanium dioxide nanoparticles allow the UVA rays to pass, resulting in reduced protection in this spectrum [20], ZnO nanoparticles provide a robust defense against both UVA and UVB radiation. ZnO with a direct band gap of approximately 3.37 eV is widely utilized across various industries including optical and electrical [21], cosmetics, dermatology, energy storage and production, and coloring [22], due to its bio-compatibility and safety profile, with its nanostructures displaying diverse morphologies that confer unique properties and applications [23, 24]. Consequently, ZnO has been frequently included in formulations of reputable cosmetic brands, where it serves multiple functions, such as the prevention of bacterial growth, skin repair, and protection against UV-induced damage [25]. Moreover, ZnO is recognized for its non-allergenic, non-comedogenic, and non-irritating properties [26]. ZnO nanoparticles can possess a varying range of band gaps, which is attributed to their crystallinity, morphology, particle size, crystallite size, and defect concentration within the crystals, particularly oxygen vacancies and zinc interstitials [27-29]. Both David et al. and Agarwal et al. confirmed that the optical band gap of ZnO nanostructures can be tuned by adjusting crystallinity, morphology, and crystallite size. Their results showed that different morphologies, such as nanoparticles and nanorods, lead to band gap variations between 3.10 and 3.37 eV, enabling the optimization of ZnO for UV-protection and optical applications [28, 29]. This variation can affect properties, including refractive index, thermal conductivity, antibacterial performance, and UV absorption. Additionally, ZnO exhibits moisturizing, antibiotic, and fragrance properties [30], making it highly valuable in cosmetic products like baby powders, sunscreens, and burn ointments [31]. ZnO nanoparticles are particularly effective in reflecting UV rays due to their uniform distribution on the skin, which helps form a comprehensive protective layer. This significantly enhances the efficacy of the formulation [17]. The Sun Protection Factor (SPF) is a standard measure for evaluating sunscreen effectiveness, and a 2018 study found that increasing ZnO concentration correlates with higher SPF values, emphasizing ZnO's critical role in sunscreen performance [7].

It is crucial to note that smaller ZnO particle sizes enhance the efficacy of UV reflection for both UVA and UVB rays [32]. Studies by Pinel's have shown that ZnO offers superior UVA protection compared to titanium dioxide [33, 34]. On one hand, ZnO nanoparticles can provide higher UV protection due to quantum mechanical effects that modify energy levels during electron transitions. On the other hand, the safety of nanoparticles has become a global concern, particularly regarding the skin absorption of ZnO nanoparticles and potential toxicity. However, the Faculty of Health and Medical Sciences at the University of Melbourne confirmed that only a minor degree of zinc ion penetration occurs, which is not expected to cause cytotoxic effects [10]. The U.S. Food and Drug Administration (FDA) has set a maximum allowable concentration of ZnO in sunscreens at 25 %. ZnO, when used in sunscreens, protects against UVA and UVB radiation via reflection and scattering, classifying it as a broad-spectrum sunscreen [35].

The research conducted by Chromik et al. on the impact of ZnO particle size revealed that particles smaller than 70 nm show increasing UV absorption with size, while particles larger than 70 nm demonstrate reduced absorption, behaving like opaque materials due to fewer particles [36]. ZnO can provide broad UV protection through three mechanisms: absorption, reflection, and scattering [8]. Absorption dominates due to ZnO's wide band gap, which enables the dissipation of absorbed UV energy as heat. This reduces the formation of free radicals, limiting oxidative stress and cellular damage. Meanwhile, particle size and morphology contribute to improved reflection and scattering [28, 37].

The primary objective of this research is to investigate the sizes and morphologies of ZnO particles, which serve as physical absorbers of UV radiation in sunscreen formulations that provide high protection against both UVA and UVB rays. To achieve this, structural characterization tests and functional evaluations were conducted to assess the efficacy of ZnO nanoparticles in the formulated sunscreens.

2. Experimental

In this study, six pharmaceutical-grade types of ZnO powders were purchased from GAM Laboratory. These powders exhibited distinct morphologies and sizes, which were analyzed using Mira III -TESCAN device for field emission scanning electron microscopy (FESEM). A TESCAN SEM device with a VEGA 3-SAMX detector was used to analyse the chemical composition of ZnO samples to record Electron dispersive spectroscopy (EDS). X-ray diffraction (XRD) patterns were recorded on a Rigaku D/max Ultima III X-ray diffractometer with Cu Ka radiation (λ= 0.15418 nm) operated at 40 kV and 150 mA at a scanning step of 0.04°. The rheological behaviour of the sunscreen creams was evaluated using an RMS/ MCR302 rheometric mechanical spectrometer (RMS). The rate of UV absorption of the samples was analyzed using a BlurAzma UV spectrometer and a Diffuse Reflectance Spectrometer SCINCO S-1400 model. The mechanical stability of the samples was tested using the Pole Ideal Tajhiz centrifuge PIT-320. A Cooling Shaking Incubator of Pole Ideal Tajhiz PIT053RS model was used to check the thermal stability. The concentrations (ppm) of heavy metals in the sunscreen creams were tested by Inductively Coupled Plasma Mass Spectrometry (ICP-MS; SPECTRO ARCOS) to assess the toxicity.

The formulation of the sunscreens comprised two phases: the aqueous phase and the oil phase, as illustrated in Figure 1 and detailed in Table 1. Six sunscreen creams were produced using the aforementioned ZnO particles, maintaining identical ingredients and production processes; the sole variation among the formulations was the type of ZnO powder employed. To evaluate the protective efficacy of the ZnO particles, a solution containing 0.01 wt. %. ZnO was prepared and subjected to an ultrasonic bath for 15 minutes. Subsequently, the absorption rates of the ZnO powders were measured using an Ultraviolet-Visible spectrometer (UV-Vis).

To evaluate the efficacy of sunscreen formulations in protecting against UV radiation, both in suspension and solid states, we employed a UV-Vis spectrometer and a DRS. To assess the protective capabilities of ZnO particles in the suspension state, a specific experimental protocol test was developed using the UV-Vis spectrometer. In this procedure, one gram of the sunscreen cream was combined with 40 mL of ethanol and 60 mL of DI water in a 100 mL beaker, and the resulting mixture was subjected to an ultrasonic bath for 5 minutes. Subsequently, the solution was filtered and diluted prior to analysis using UV-Vis spectroscopy. To determine the protective efficacy of ZnO particles in the solid state, a diffuse reflectance spectrometer was employed. In this part of the study, the sunscreen creams were applied to the sample holder of the spectrometer, and the level of UV protection was quantified.

To assess the acidity and alkalinity of the produced creams, a suspension was prepared with a 10 wt. % concentration of water, and the pH of the samples was measured using a pH meter. To evaluate the structural stability of the sunscreen creams under varying environmental conditions and during transportation, mechanical stability was assessed by placing 5 grams of each sample in a Falcon tube and centrifuging at 5000 rpm for 30 minutes. Additionally, to examine the appearance of the creams over a period of 6 to 24 months at ambient temperature, thermal stability was evaluated using an incubator in accordance with standard protocols [32]. A rheometric mechanical spectrometer (RMS) test was conducted to assess the viscosity of the creams and analyze their rheological behavior.

Table 1: Formulation of sunscreen cream.

Oil Phase	Amount (Wt. %)	Aqueous Phase	Amount (Wt. %)
water	46	Stearic acid	2.6
Glycerin	4	Cetyl alcohol	2.2
Propanediol	5	Shea butter	1.5
Sorbitol	1	Dimethicone	0.2
EDTA	0.1	Beeswax	1.6
Propylene glycol	1	GMS	2.3
ZnO	15	Isopropyl palmitate	4.5
Xanthangam	0.1	Polybutene	0.1
Panthenol	0.5	Stearate 20	0.4
Caprylic capric triglyceride	7	Lanolin	1.5
TEA	0.3	Palmitic acid	1.6
		Jojoba oil	1.5

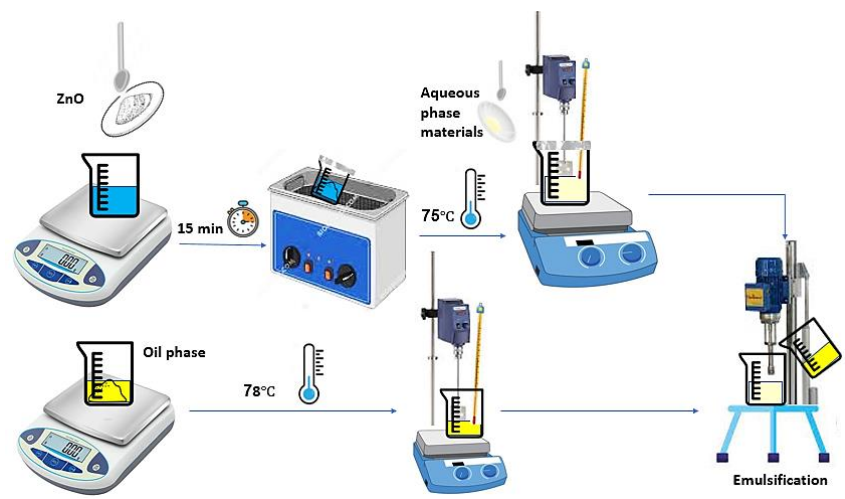

Figure 1: Schematic of the sunscreen production process.

3. Results and Discussion

3.1. ZnO nanoparticles

3.1.1. Microscopic study

Figure 2 a-f shows several FE-SEM images of the ZnO samples. All six ZnO samples displayed distinct morphologies and particle sizes. The morphologies of samples Z1, Z2, and Z3 are characterized as plate-like, spherical, and irregular, respectively. The Z1 sample demonstrates an average plate width of 71 nm and an average length of 214 nm. The Z2 sample exhibits an average diameter of 40 nm, while the irregular particles of sample Z3, predominantly rod-shaped, possess an average dimension of 66 nm. The morphologies of samples Z4, Z5, and Z6 are classified as plate-like, hedgehog-shaped, and plate-like, respectively. The Z4 sample has an average width of 42 nm and an average length of 164 nm. For the Z5 sample, which contains the hedgehog-shaped particles, the average diameter of the hedgehog structures is 840 nm, with an average blade length of 162 nm and an average diameter of 52 nm. Finally, the Z6 sample exhibits an average width of 40 nm and an average length of 148 nm.

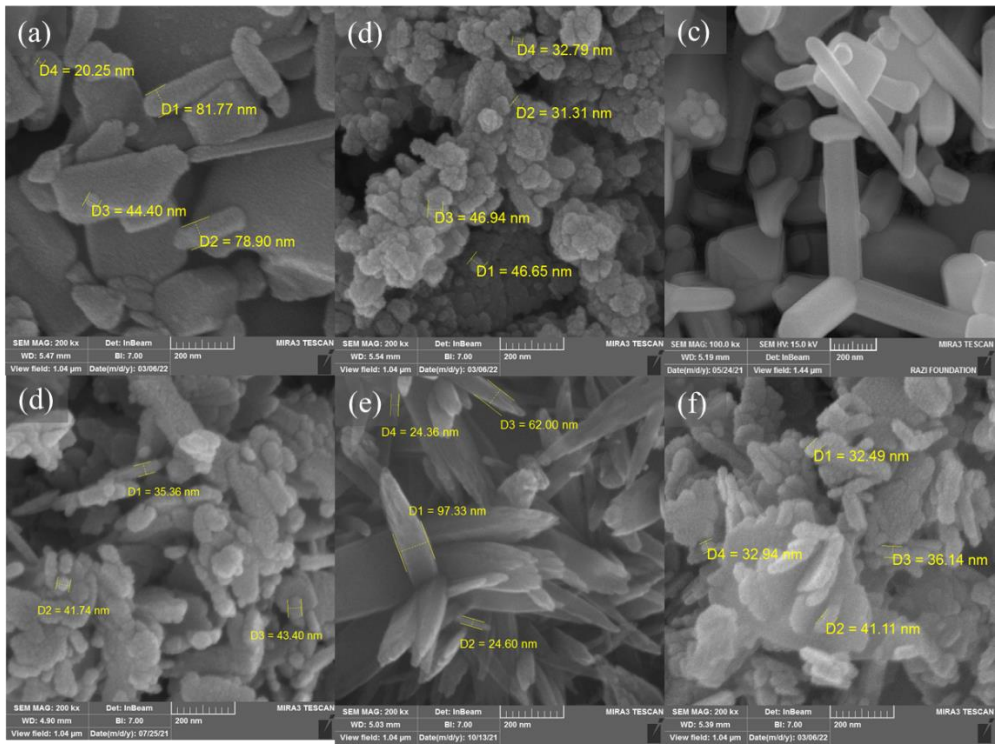

Figure 2: Microscopic images at 200nm and 1 µm scale respectively of the microstructure of ZnO by FE-SEM, a) Z1, b) Z2, c) Z3, d) Z4, e) Z5, and f) Z6.

Zinc oxide typically exists as a single stable stoichiometric phase, ZnO, under ambient conditions. Although zinc-rich phases such as Zn_2O are sometimes discussed theoretically, they are not recognized as stable crystalline phases. It is worth noting that they possess different crystalline parameters. Therefore, to ensure that all the samples in this work are pure ZnO and to eliminate the possibility of the presence of Zn_2O or other non-stoichiometric phases, X-ray diffraction (XRD) analysis was performed, and the patterns obtained are given in Figure 3. Phase identification using E'xpert Highscore software ensured that the diffraction peaks refer to the hexagonal wurtzite structure of ZnO, in agreement with ICSD reference code 065120 [37, 38]. ZnO, if present, would have quite dissimilar lattice constants and a different crystal structure, which were not detected. In order to further validate the phase purity, lattice parameters (a, b, and c) were calculated from multiple characteristic diffraction peaks of each sample using Bragg's law and the Nelson-Riley extrapolation technique, as shown in equations 1 and 2 and presented in Table 2.

$$n\lambda = 2dsin\theta \quad (1)$$

$$\frac{1}{d^2} = \frac{4}{2}\left(\frac{h^2+hk+k^2}{a^2}\right) + \frac{l^2}{c^2} \quad (2)$$

Table 2: Lattice parameters (a, b and c) calculated from characteristic diffraction peaks of samples.

Sample	a (Å)	b (Å)	c (Å)
Z1	3.2489	3.2489	5.2083
Z2	3.2429	3.2429	5.1929
Z3	3.2399	3.2399	5.1852
Z4	3.2459	3.2459	5.2006
Z5	3.2519	3.2519	5.2161
Z6	3.2549	3.2549	5.2239

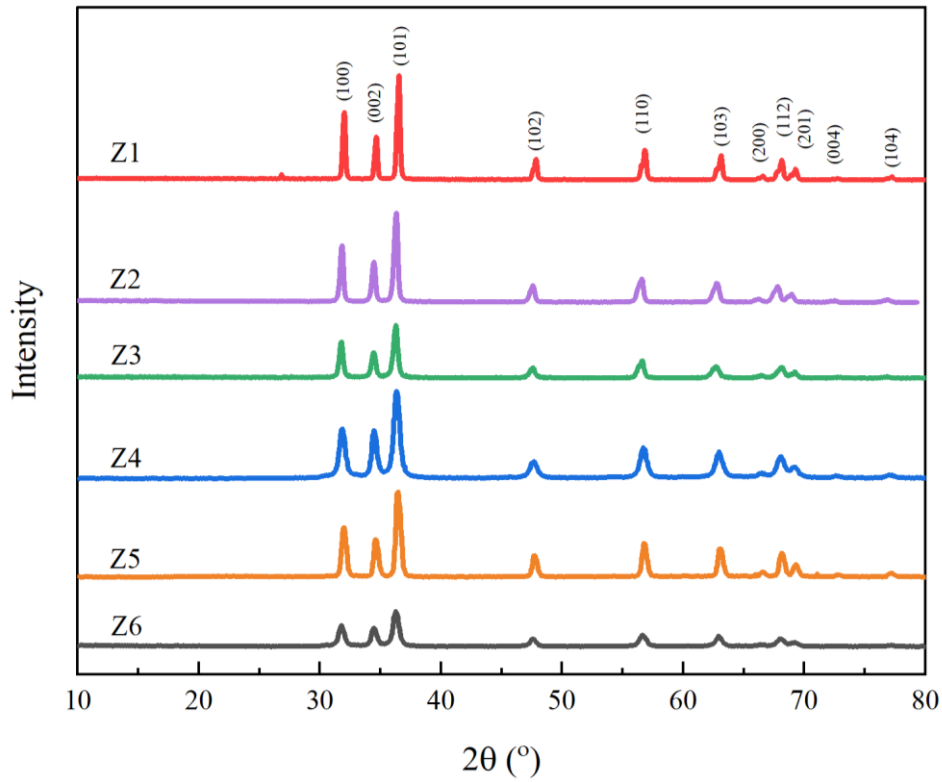

Figure 3: XRD pattern of Z1, Z2, Z3, Z4, Z5, and Z6 samples.

Table 3: X-Ray energy dispersive spectroscopy (EDS) results.

Sample		Z1	Z2	Z3	Z4	Z5	Z6
Atomic%	Zn	34.41	24.74	31.32	33.10	32.46	33.52
	O	65.59	75.26	68.68	66.90	67.54	66.48

The results show values consistent with literature data for pure ZnO, slightly deviating due to infinitesimal defect densities or internal strain, which is due to the employed synthesis methods. No sign of the more general structural distortions that would imply Zn_2O formation was detected, thereby confirming the exclusive presence of the ZnO phase in all the samples [28, 39, 40].

Table 3 presents the results of the EDS analysis. The EDS results for the ZnO powders show that all ZnO particles exhibit high purity, comprising solely of zinc and oxygen atoms. However, as discussed, EDS has known limitations in accurately quantifying light elements such as oxygen and cannot detect interstitial atoms. Moreover, the technique is sensitive to surface contamination, adsorbed oxygen species, and preferential sputtering, all of which can contribute to deviations from the ideal Zn:O ratio. Nevertheless, previous studies have demonstrated that, despite these limitations, the Zn:O ratio obtained from EDS analysis can still serve as a useful comparative parameter when evaluating different samples. Variations in the Zn:O ratio can be correlated with the relative concentration of defects such as zinc interstitials or oxygen vacancies. Therefore, based on these considerations, together with the XRD results and the information provided in Table 3, it can be inferred that the observed deviations reflect differences in defect structures among the samples rather than solely being due to surface effects.

3.1.2. UVR protection efficacy

The mechanism by which ZnO nanoparticles protect the skin from UV radiation involves processes of absorption, reflection, and scattering [8]. Figure 4a illustrates the absorption spectrum of six ZnO samples within the UVB

region, while Figure 4b presents the absorption spectrum in the UVA region, as measured using a UV-Vis spectrometer. The peak was observed at a wavelength of 377 nm, as depicted in Figure 4b, which corresponds to electron excitation within the energy gap of ZnO [36]. The existence of an energy gap in the UVA region facilitates the absorption of UV radiation. Specifically, the absorption exhibited by ZnO nanoparticles is attributable to this energy gap within the UVA range. Since UVA rays are associated with an increased risk of skin cancer over prolonged exposure, the utilization of zinc oxide as a UV ray absorber is deemed appropriate for long-term protection against skin cancer.

The absorption mechanism is attributed to the existence of an energy gap, which is further elucidated by the presence of structural defects. Additionally, the mechanisms of reflection and scattering play a crucial role in providing protection against UV radiation. The morphology and size of ZnO particles significantly influence these two mechanisms. A morphology characterized by a higher surface area offers an increased contact surface, thereby enhancing the possibility of scattering and reflection in response to UV radiation, which correlates with improved protective capabilities. As illustrated in Figure 4a, the Z1 sample exhibits the highest absorption, followed by the Z6 and Z4 samples, all of which display a plate-like morphology. It is observed that the absorption capacity increases with the increase in the size of the nanoparticles, reaching a maximum at 70 nm [36]. Specifically, the Z1 sample has a plate width of 71 nm, while the Z6 and Z4 samples have plate widths of 42 and 40 nm, respectively. The Z5 sample, which possesses a hedgehog-shaped morphology, the Z3 sample with an irregular (predominantly rod-like) morphology, and the Z2 sample with a spherical morphology demonstrate lower absorption levels in that order. The enhanced absorption observed in the Z5 and Z3 compared to the Z2 samples can be attributed to the intrinsic properties of their respective materials. Consequently, the energy gap, morphology, and dimensions collectively influence the overall performance of UVA protection.

In the UVB range, the absence of an energy gap results in a lack of electron excitation peaks within the energy gap. The UVB rays protection is achieved through two primary mechanisms: reflection and scattering, which are influenced by two critical factors: the morphology and dimensions of the ZnO particles. When planar particles are aggregated, they present a larger surface area for reflection and scattering, leading to the highest absorption levels observed in the Z1, Z4, and Z6 samples. Among these three samples, which share the same morphology, an increase in the size of the plates correlates with an enhanced surface area for reflection and scattering, thereby improving the level of protection. Notably, absorption increases with particle size up to 70 nm, as indicated before [36]. Furthermore, in the case of the Z2 sample, which exhibits spherical morphology, the irregular and hedgehog-like close packing of particles results in a greater contact surface area compared to the Z3 and Z5 samples. Consequently, the Z2 sample demonstrates commendable absorption, ranking just below the Z1, Z4, and Z6 samples.

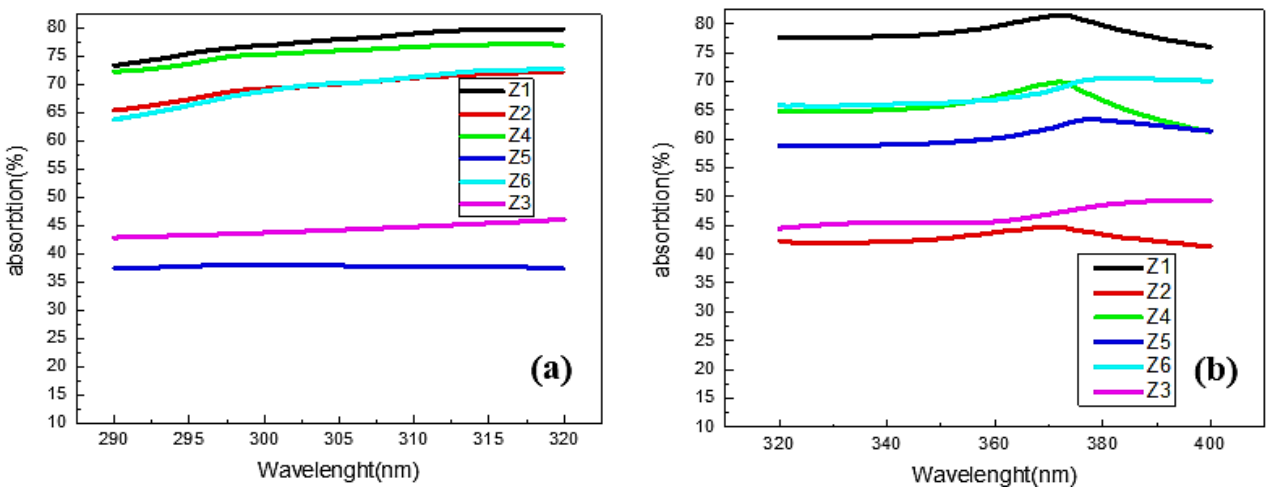

Figure 4: UV absorption of ZnO powder within a) UVB region and b) UVA region.

In the irregular particles of the Z3 sample, the ability to occupy voids with smaller particles results in an increased covered surface area compared to the hedgehog morphology observed in the Z5 sample. Consequently, the potential for reflection and scattering of ultraviolet rays in the Z3 sample is greater than that in the Z5 sample, indicating that the Z3 offers superior protective qualities.

In the Z5 sample exhibiting a hedgehog morphology, characterized by blades that are interwoven, there exists a potential for tunneling between the blades. However, this particular morphology results in a reduced surface area available for the reflection and scattering of incident rays. Consequently, given that the primary protective mechanism against UVB radiation relies on reflection and scattering, the Z5 sample demonstrates a lower level of protection in comparison to the other samples.

3.1.3. Band gap measurement

The energy gap refers to the energy difference between the conduction band and the valence band. More specifically, it represents the energy required to promote an electron from the valence band to the conduction band. Figure 5 shows the energy gaps of six ZnO samples, which were determined using the Tauc method [27].

The observed differences in energy gap values among the various samples can be attributed to structural defects, including vacancies and interstitials, present within the ZnO crystal structure. Such structural defects can create localized energy states within the bandgap, thereby influencing the energy required for electron excitation. Generally, Samples exhibiting fewer structural defects will possess a larger energy gap, as there are fewer intermediate energy states available for electron occupancy. In contrast, samples characterized by a higher density of structural defects will demonstrate a reduced energy gap, as the energy states induced by these defects facilitate electron excitation at lower energy levels. The variation in bandgap energy across the different ZnO samples is a critical factor, as it significantly affects bandgap energy impacts the material's optical and electronic properties, ultimately determining its suitability for various applications. According to the studies, an increase in zinc vacancies and oxygen interstitials correlates with a decrease in the energy gap [27]. Table 4 presents the energy gap values for six ZnO samples. Notably, the energy gap for all samples is lower than the energy gap of the bulk ZnO sample, which is 3.36 eV. This reduction is attributed to the structural defects present in the samples [27]. Furthermore, as indicated in Table 3 and Table 4, there is a consistent trend where an increase in zinc vacancies and oxygen interstitials results in a decrease in the energy gap across the ZnO samples. Specifically, the Z2 sample exhibits the highest concentration of zinc vacancies and oxygen interstitials, resulting in the lowest energy gap. In contrast, the Z3, Z5, Z4, Z6, and Z1 samples display progressively lower concentrations of zinc vacancies and oxygen interstitials, leading to an increase in the energy gap in the order specified.

Consequently, the Z1 sample, which exhibits the lowest concentration of zinc vacancies and oxygen interstitials, possesses the largest energy gap. Previous studies have indicated that the presence of zinc vacancies and oxygen interstitials can reduce the energy gap of zinc oxide by 2.1 and 2.6 eV, respectively. Figure 6 shows the reduction of the energy gap attributable to structural defects in ZnO. The increase in oxygen intercalation leads to the formation of an intermediate gap between the energy levels, ultimately resulting in a decrease in the overall energy gap [41].

Table 4: Energy gap of zinc oxide samples.

Sample	Z1	Z2	Z3	Z4	Z5	Z6
Energy gap (ev)	3.12	2.63	2.81	3.01	2.94	3.04

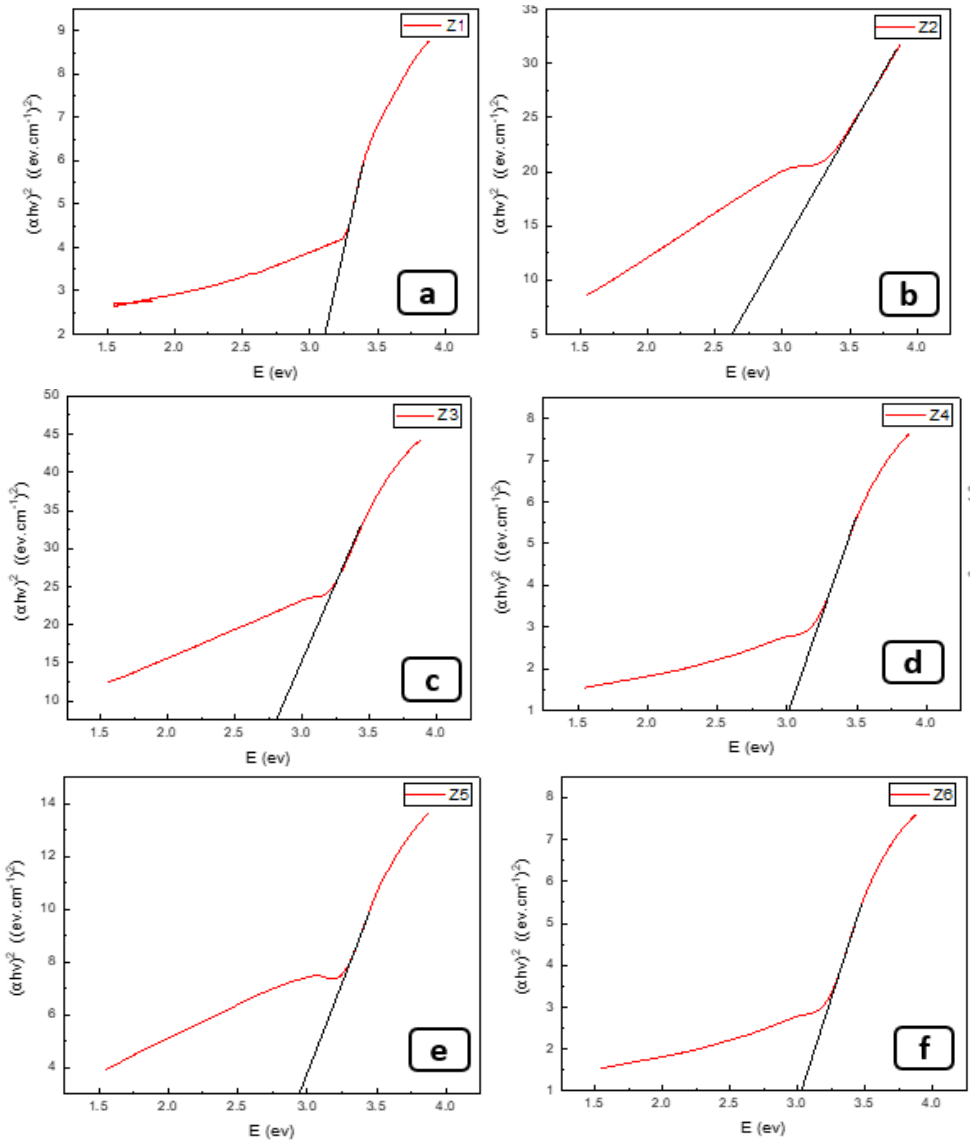

Figure 5: Energy gap of zinc oxide samples a) z1, b) Z2, c) Z3, d) Z4, e) Z5, and f) Z6.

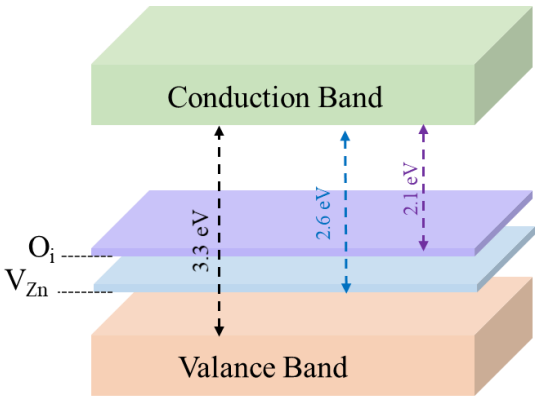

Figure 6: Energy gap reduction by structural defects in ZnO.

3.2. Sunscreen creams evaluation

Sunscreen formulations incorporating ZnO nanoparticles were subjected to a series of functional evaluations. These assessments included the examination of toxicity related to heavy metal ions, stability, rheological properties, and the protective level against ultraviolet radiation. A detailed discussion of these evaluations will be presented in the following sections.

3.2.1. Toxicity

Heavy metals are recognized as environmental pollutants that can induce toxicity in cosmetic products. Consequently, regulatory limits for heavy metal concentrations in cosmetic products have been established to ensure their safety for consumers. FDA has set the permissible concentration of mercury in cosmetic products at 1 ppm and that of arsenic at 3 ppm. The Analysis of the samples using ICP analysis indicates that all tested products contain mercury levels significantly below the established limit. In terms of arsenic content, samples Z1 and Z6 meet the permissible threshold, while the remaining samples exhibit concentrations lower than the specified limit. Therefore, the presence of heavy metals is deemed acceptable in the allowed in six sunscreen samples analyzed. Table 5 shows the concentrations of mercury and arsenic found in the sunscreen formulations.

3.2.2. Stability

Cosmetic products must possess a certain shelf life and demonstrate stability to endure the various conditions they may encounter, including transportation from the manufacturing facility and storage conditions in retail environments. To this purpose, the stability of sunscreen creams was examined in two distinct aspects, including thermal stability and mechanical stability.

The thermal stability of the samples was assessed to evaluate in order to investigate the useful life of the sunscreen formulations. In accordance with established standards [32], the samples were maintained in an incubator at a temperature of 45°C under ambient humidity conditions for a duration of one month. All sunscreen samples exhibited stability throughout this thermal stability assessment. Figure 7a illustrates the sunscreen samples within the incubator, while Figure 7b shows the sample after one month at 45 °C. This evaluation of thermal stability is crucial in ensuring that the creams can withstand anticipated temperature fluctuations during storage and transportation, thereby preserving their intended properties throughout the designated shelf life.

Furthermore, Table 6 shows the pH values of the sunscreen samples produced, both prior to and following thermal stability tests. Based on the observed pH variations, it can be inferred that the samples exhibit chemical stability, maintaining the pH approximately equal to 7. The literature indicates that the optimal pH range for sunscreen formulations is between 6.8 and 7.5 [42].

Table 5: Concentrations of heavy metals in sunscreen samples.

Sample	Z1	Z2	Z3	Z4	Z5	Z6
As (ppm)	3.01	2.48	1.47	0.83	1.79	3.03
Hg (ppm)	<0.10	<0.12	<0.10	<0.10	<0.10	<0.10

Table 6: pH changes of sunscreen samples prior to and following thermal stability tests.

sample	Z1	Z2	Z3	Z4	Z5	Z6
pH prior to the stability test	7.15	7.21	7.19	7.55	7.19	7.22
pH following the stability test	7.06	7.13	7.12	7.44	7.13	7.16

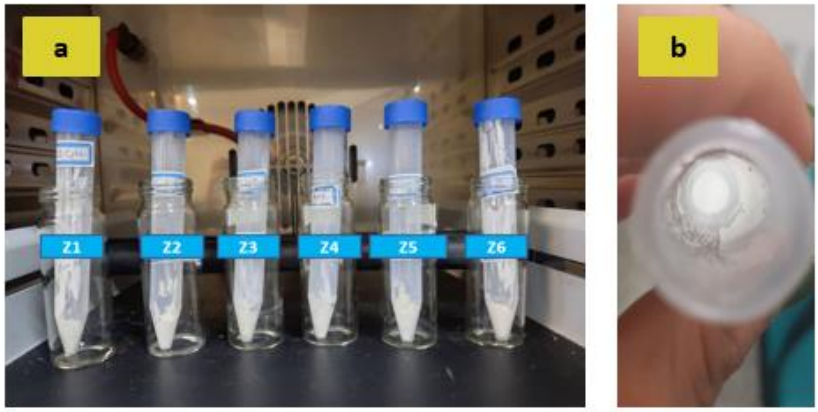

Figure 7: a) The sunscreen sample produced using Z1, Z2, Z3, Z4, Z5, and Z6 samples inside the incubator, and b) a digital image with higher zoom showing the stability of a representative sample after one month at ambient temperature.

In addition to evaluating thermal stability, the mechanical stability of the sunscreen samples was assessed to determine their useful life. The mechanical stability test was conducted in accordance with standard protocols, wherein the samples were subjected to centrifugation at a speed of 5,000 rpm for a duration of 30 minutes [43]. Figure 8 presents the images from the mechanical stability testing of the produced sunscreen samples. All the samples demonstrated adequate mechanical stability and did not exhibit any structural changes within the emulsion, indicating their ability to withstand the mechanical stresses encountered during transportation, such as shipping and handling.

3.2.3. Rheological behavior

In order to investigate the variations in viscosity behavior and shear stress across different shear rates, three representative samples (Z1, Z3, and Z5) were selected from the sunscreen samples for analysis using Rheometric Mechanical Spectroscopy (RMS). Figure 9 illustrates the viscosity and shear stress profiles of three selected sunscreen samples across various shear rates. This rheological analysis provides valuable insights into the flow and deformation characteristics of the sunscreen formulations. A comprehensive understanding of the rheological properties is crucial, as it ensures that the creams possess the requisite viscosity and flow behavior for effective application and spreadability on the skin, while also preserving structural integrity during storage and use.

Sample Z5 exhibited the highest initial shear stress at 900 Pa, indicating that it requires a greater amount of stress to initiate flow and mixing in comparison to samples Z3 (640 Pa) and Z1 (125 Pa). For sample Z5, at a shear rate of 500 (1/s) and a shear stress of 0.15 Pa, there was a significant decrease in shear stress as the shear rate increased. This observation indicates a disruption of the network structure within sample Z5, which demonstrates shear-thinning behavior. In contrast, samples Z1 and Z3 displayed Newtonian flow behavior, characterized by a constant viscosity regardless of changes in shear rate. Sample Z5, however, exhibited non-Newtonian shear-thinning behavior, wherein viscosity decreases as the shear rate increases.

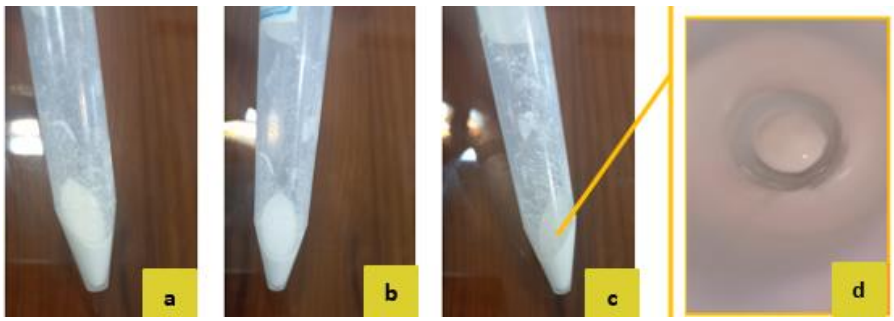

Figure 8: Digital images of the produced sunscreen samples after mechanical stability testing, and d) a digital image with higher Magnification showing the stability of a representative sample.

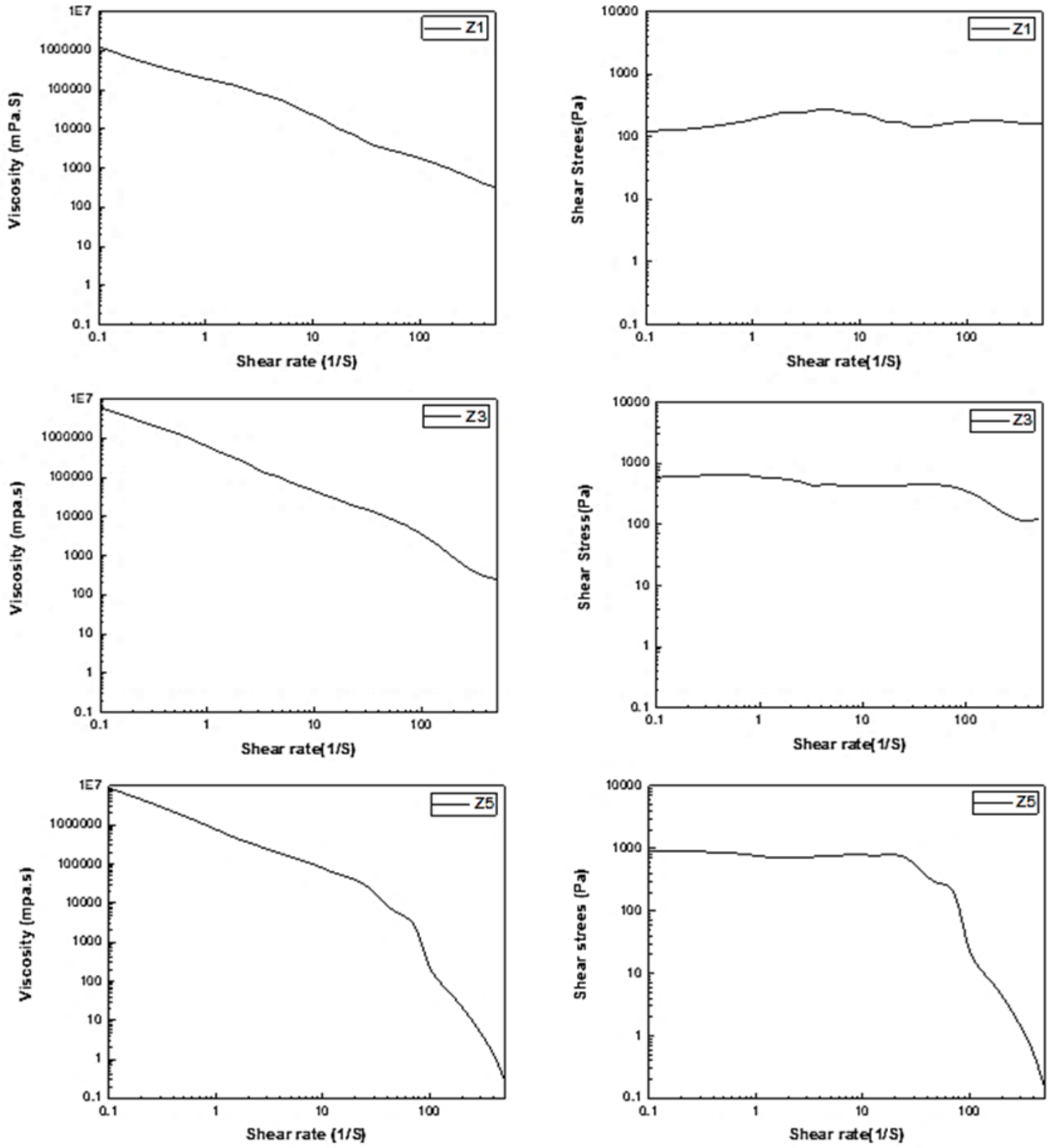

Figure 9: Change of shear stress (right images) and viscosity (left images) according to shear rate changes for samples Z1, Z3, and Z5.

Initially, an entanglement of particles occurs, resulting in the formation of a network structure under conditions of high shear stress. As the shear rate increases, specifically around 25 1/s for sample Z5, the connections between the open nanoparticles and the network become disrupted, which leads to a reduction in shear stress. This disruption of the network structure results in the non-linear, shear-thinning behavior observed in sample Z5. This thorough comprehension of the rheological properties, particularly the shear-thinning mechanism, provides valuable insights into the structural characteristics and flow behavior of various sunscreen cream formulations.

In the three sunscreen samples analyzed (Z1, Z3, and Z5), ZnO nanoparticles serve as the only reinforcing agent, with a consistent quantity of ZnO

present across all samples. However, the morphologies and sizes of the ZnO nanoparticles vary among these samples. The variation in morphology is likely responsible for the observed differences in the rheological behavior of the samples, including shear stress and viscosity. Sample Z5, which contains ZnO nanoparticles exhibiting a hedgehog morphology, demonstrated the highest shear stress and viscosity. Sample Z3, characterized by irregular (mostly rod-shaped) ZnO nanoparticles, displayed intermediate levels of shear stress and viscosity. Finally, sample Z1, containing plate-like ZnO nanoparticles, showed the lowest shear stress and viscosity. These findings suggest that the morphology of ZnO nanoparticles, along with the degree of particle entanglement, is a critical factor in determining the rheological properties of sunscreen formulations, even when the concentration of nanoparticles remains constant.

The analysis of nanoparticle sizes reveals that as the sizes increase, both viscosity and shear stress exhibit a decreasing trend. This phenomenon can be attributed to a reduction in particle entanglement. Consequently, sample Z5, which demonstrates the highest shear stress and viscosity, possesses an average dimension of 52 nm, whereas sample Z1, characterized by the lowest viscosity and shear stress, has a dimension of 71 nm. In sample Z1, the initial shear stress is relatively low, and as the shear rate increases, there is no significant change in shear stress, indicating the absence of transverse connections within this sample. Conversely, samples Z3 and Z4 exhibit elevated shear stress at the initial shear rate, and as the shear rate increases, the shear stress also rises, suggesting the formation of a network structure in both samples. This network acts as a hindrance to fluidity; in sample Z5, at an approximate shear rate of 500 1/s, both viscosity and shear stress experience a substantial reduction, reaching approximately 0.15 Pa, which indicates the failure of the network structure.

3.2.4. UV protection behavior (UV-Vis)

The present study investigated the protective behavior against UV radiation in both suspension and solid-state formulations, utilizing UV-Vis spectroscopy and DRS analysis. The integration of UV-Vis spectroscopy and DRS analysis provides a comprehensive approach for assessing the UV protection properties of sunscreen formulations in both suspension and solid states. This approach facilitates the optimization of these formulations for enhanced UV shielding efficacy.

The analysis conducted through UV-Vis spectroscopy offers valuable insights into the UV protection capabilities of sunscreen samples. This technique quantifies the absorbance of the samples across the UV and visible light wavelength ranges, thereby facilitating the evaluation of their efficacy in blocking harmful UV radiation. Two primary parameters that influence the UV absorption characteristics of ZnO particles in sunscreen formulations are the concentration of ZnO and the specific type of ZnO utilized. Figure 10 illustrates the UV absorption characteristics of the sunscreen samples. The samples Z1, Z4, and Z6, which display a plate-like morphology, demonstrate a higher absorption rate in comparison to the other samples.

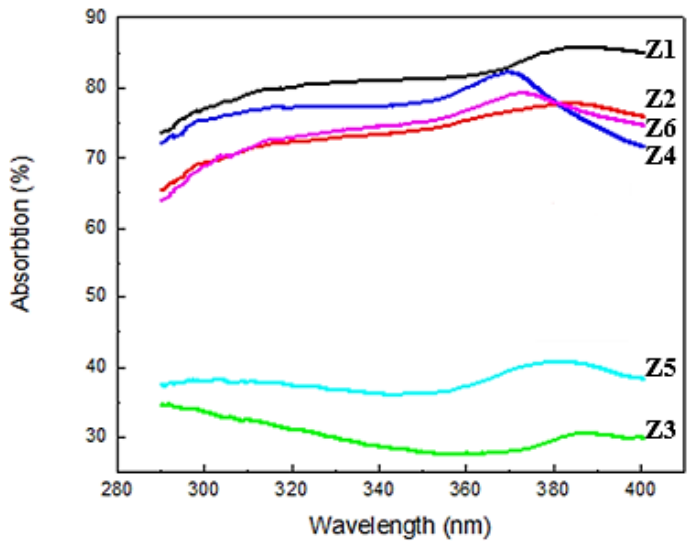

Figure 10: Investigating the level of protection of sunscreen creams with different ZnO.

According to the literature [36], for samples exhibiting the same morphology, the UV absorption rate increases as the particle size increases within the range of 40-70 nm. The enhanced UV protection offered by plate-like samples can be attributed to their larger surface area, which facilitates more effective reflection and scattering of UV radiation.

The Z2 sample, characterized by a spherical morphology with an average dimension of 40 nm, demonstartes significant UV absorption; however, it does not exhibit as much absorption as the plate-like samples (Z1, Z4, Z6). In comparison to the Z3 and Z5 samples, the Z2 sample offers a greater contact surface area for the reflection and scattering of UV rays, which contributes to its enhanced UV absorption. Although the Z3 sample, which possesses an irregular and predominantly rod-like morphology with an average dimension of 66 nm, has a larger contact area than the Z5 sample, the latter (exhibiting a hedgehog morphology with an average dimension of 52 nm) shows superior UV absorption. This phenomenon can be attributed to the hedgehog-like structure of the Z5 sample, which, despite comprising smaller individual particles, provides a more extensive overall contact surface area for UV reflection and scattering in comparison to the irregular rod-like structure of the Z3 sample. In conclusion, the UV absorption performance of the samples is influenced by both particle morphology and dimensions.

The FDA has established a maximum allowable concentration of ZnO in sunscreen formulations at 25 %. However, increasing the ZnO concentration beyond 21 wt. % results in a heavier texture and an undesirable white appearance on the skin. This study investigates the effect of ZnO concentrations up to 21 wt. % was investigated. Figure 11 illustrates the protective efficacy of sunscreen creams with varying concentrations of ZnO. It is important to note that all samples examined samples in Figure 11 contain a single type of ZnO (designated as sample Z1), indicating that only the concentration of ZnO in the cream influences the observed effects.

The results indicate that increasing the concentration of ZnO from 10 to 12 wt. % leads to a significant enhancement in absorption. Additionally, as the concentration of ZnO is further increased to 15 wt. %, the absorption approaches nearly 85 %. However, upon increasing the ZnO concentration to 18 wt. %, a decline in absorption is observed, which continues to decrease as the concentration rises to 21 wt. %. This phenomenon can be attributed to the fact that higher concentrations of ZnO result in increased viscosity and alterations in the optical properties of the sunscreen [44]. It is important to note that the type of ZnO used in the five samples examined was consistent, the morphology and particle size remained unchanged; thus, only the concentration of the nanoparticles influences the optical properties.

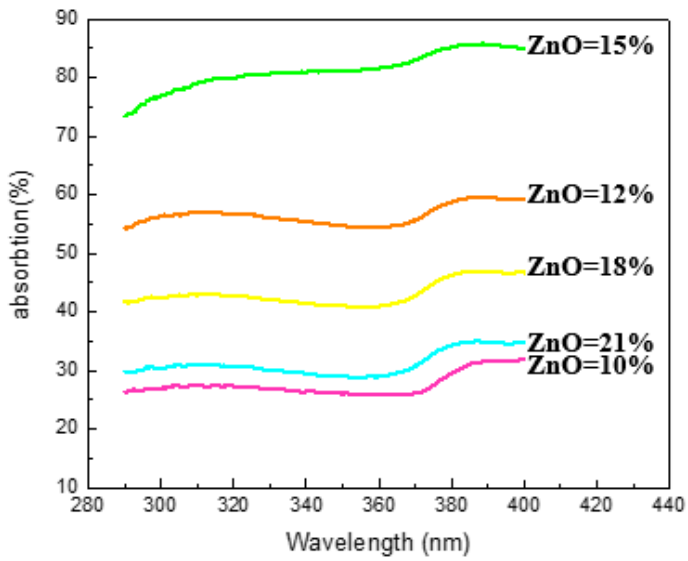

Figure 11: Investigation of the protective efficacy of sunscreen creams with varying concentrations of ZnO.

Increasing the concentration of ZnO from 10 to 12 wt. % enhances the inter-particle contact, leading to the formation of clusters. As the ZnO concentration is further elevated to 15 wt. %, the particles achieve maximal contact with adjacent particles, resulting in the establishment of a permeation network of nano-particles that approaches the critical concentration of the reinforcements. It is possible that a slight increase in ZnO concentration to 15 wt. % may yield a marginal enhancement in absorption. However, upon further increasing the concentration to 18 wt. %, the system reaches a supersaturated state, causing the ZnO particles to aggregate and form lumps. Consequently, the overall contact surface area diminishes, and the particle size increases. An additional rise in ZnO concentration leads to a decrease in absorption, attributable to the aggregation of particles and their increased dimensions. Research indicates that when particle dimensions exceed 70 nm, the absorption capacity declines [25].

3.2.5. UV protection behavior (DSR)

To ensure the accuracy of the data obtained regarding the protective efficacy of sunscreen formulations with varying ZnO concentration, the degree of protection was assessed using DRS analysis. Figure 12 shows the protection levels of sunscreen formulations with differing ZnO concentrations, as quantified by DRS. As depicted in Figure 12, an increase in ZnO concentration from 15 to 18 wt. % correlates with a decrease in protective efficacy. Furthermore, as the concentration of ZnO continues to rise, this reduction in protection becomes increasingly pronounced. Consequently, the DRS data corroborate the obser-vation that exceeding the critical concen-tration of ZnO (15 wt. %) leads to a supersaturated state within the formulations, resulting in the aggrega-tion of particles subsequent decline in protective efficacy.

3.2.6. Commercialercial evaluation

In order to evaluate the efficacy of UV ray protection, a comparative analysis was conducted between the sunscreen produced in this study and various commercial samples. Figure 13 shows the comparison between the commercial samples and the Z1 sample, which exhibited the highest absorption rate among the produced formulations. As shown in Figure 13a, despite the presence of multiple UV absorbers (both physical and chemical) in the commercial samples, the Z1 sample, which solely contains ZnO particles as a physical absorber, is positioned between two commercial samples with SPF of 50 and 22, respectively. This finding underscores the significant level of protection afforded by the Z1 sample.

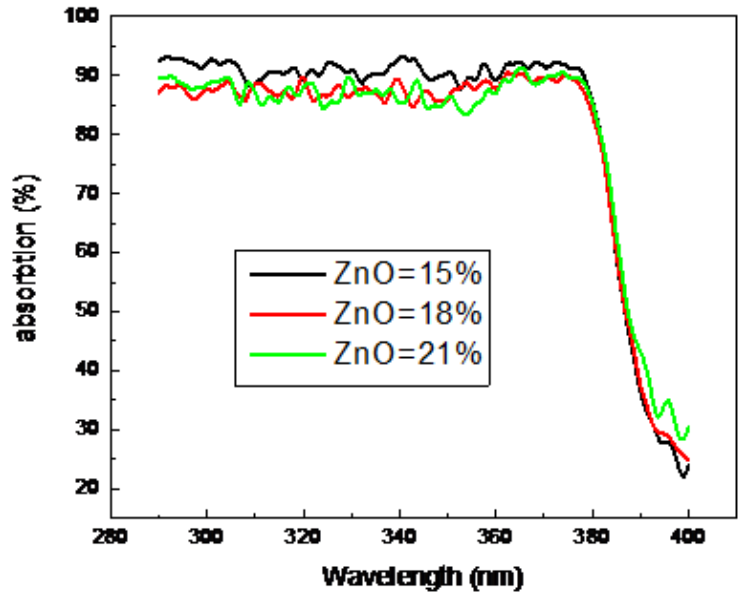

Figure 12: Investigation of the level of protection of sunscreen creams with different amounts of zinc oxide by DRS.

In Figure 13b, a comparative analysis was conducted utilizing DRS analysis, revealing that the protection level of the Z1 sample is positioned between two commercial samples with SPF of 30 and 60. Furthermore, the protection level of the Z1 sample is closely aligned with that of sunscreen products containing various chemical and physical UV absorbers. This finding underscores the substantial influence of parameters such as morphology, size, and concentration of ZnO nanoparticles within the formulation.

3.2.7. Sun protection factor

The SPF is a standardized metric used to evaluate the efficacy of sunscreen products. In this study, the SPF was determined using an in-vitro methodology. The calculation of SPF values was conducted in accordance with Equation 3 [7]. In this equation EE(λ) represents erythema effect spectrum, I(λ) is solar intensity spectrum, Abs (λ) is the absorbance of sunscreen, and CE is the correction factor. To ensure the precision of the SPF calculations, multiple commercial sunscreen samples were analyzed using UV-Vis spectroscopy and DRS analysis. The Table 7 presents the amount of the CF for the commercial samples, along with the determination of the SPF for the Z1 sample.

$$SPF = CE \times \int_{290}^{320} EE(\boldsymbol{\lambda}) \times I(\boldsymbol{\lambda}) \times Abs\ (\boldsymbol{\lambda}) \qquad (3)$$

In the analysis of commercial samples, the CE was determined using data pertaining to the intensity of the solar spectrum, the degree of absorption exhibited by the samples, and the SPF values supplied by the manufacturers. The CE for all commercial samples was identified to fall within the range of 10 to 11. Subsequently, the SPF for the Z1 sample, which exhibited the highest absorption rate among the produced samples, was calculated using the average CE of 10.530 established for the commercial samples.

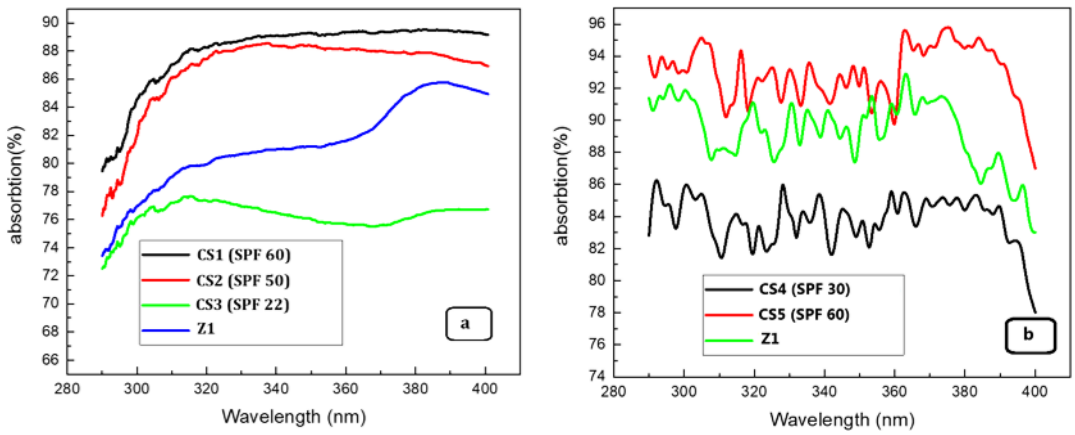

Figure 13: Comparative analysis of the protective efficacy in the produced samples and commercial samples utilizing a) UV-Vis and b) DRS analysis methods.

Table 7: Investigation the correction coefficient of commercial samples and determining the SPF of Z1 sample.

Sample	$\int_{290}^{320} EE(\lambda) \times I(\lambda) \times Abs\ (\lambda)$	CE	SPF
CS5	5.472	10.964	60
CS2	4.637	10.782	50
CS6	3.836	10.426	40
CS4	2.960	10.132	30
Z1	4.418	10.530	47

The resulting SPF value for the Z1 sample was determined to be 47. According to prior research [7, 45, 46], this value represents the highest SPF achievable for sunscreens that utilize ZnO as the sole physical UV absorber. This calculation underscores the potential for formulating a highly effective sunscreen sample (Z1) through thorough control of parameters such as particle size, particle morphology, and ZnO concentration in sunscreen formulations.

4. Conclusion

Given the detrimental effects of ultraviolet radiation on the skin, the application of physical sunscreens is strongly advocated. Zinc oxide (ZnO) serves as an effective physical ultraviolet (UV) absorber, offering substantial protection. A comprehensive regulation of parameters such as morphology, particle size, and concentration of ZnO can enhance its efficacy as a physical sunscreen component.

The findings indicate that the viscosity of the sunscreen samples increases in correlation with the morphological entanglements and particle size of zinc oxide (ZnO). A greater reflective surface area produced by the ZnO particles corresponds to an enhanced level of ultraviolet (UV) protection. There exists a direct relationship between the concentration of ZnO and the UV protection, which remains effective up to approximately 15 weight percent (wt. %). Beyond this concentration, the likelihood of agglomeration escalates, and the average particle size surpasses the optimal range, resulting in a reduction of UV protection. Notably, Sample Z1, characterized by a plate-like morphology and an average particle size of 71 nm, demonstrated the highest sun protection factor (SPF) of 47. The Z1 sample appears to possess the optimal characteristics necessary to maximize UV protection across the UVA and UVB spectra.

Acknowledgment

The authors gratefully appreciate the financial support from AmirKabir University of Technology. We sincerely appreciate the cooperation and help of our colleagues at the GAMLab. (Graphical abstract publishing permission: Created in BioRender. (2025))

5. References

1. Al-Sadek T, Yusuf N. Ultraviolet radiation biological and medical implications. Curr Issues Mol Biol. 2024; 46(3):1924-42.https://doi.org/10.3390/cimb46030126.
2. Kaur K, Ai R, Perry AG, Riley B, Roberts EL, Montano EN, et al. Skin cancer risk is increased by somatic mutations detected noninvasively in healthy-appearing sun-exposed skin. J Invest Dermatol. 2024; 144(10): 2187-2196.e13. https://doi.org/10.1016/j.jid. 2024.02.017.
3. Safapour S, Shabbir M, Rather LJ, Assiri MA. Cleaner sustainable route to develop UV protective and colorful wool yarns: natural flavonoid-based colorants from millettia laurentti sawdust. Prog Color Colorant Coat. 2024;17(4):351-63. https://doi.org/10.1016/j. jid. 2024.02.017.
4. Amnuaikit T, Boonme P. Formulation and characterization of sunscreen creams with synergistic efficacy on SPF by combination of UV filters. J Appl Pharm Sci. 2013;3(8):1-5. https://doi.org/10.1016/j.jid.2024. 02.017.
5. Sharma N, Srivastava S, Singh A, Sheikh J. Novel route for dyeing of cotton with turmeric for imparting mosquito repellent and UV protection properties. Prog Color Colorant Coat. 2024; 17(3): 289-96. https://doi. org/10.1016/j.jid.2024.02.017.
6. Musa KM, Alshemary KKH. The role of nanoparticles in sunscreen: UV protection and particle size. Int Acad J Sci Eng. 2024;11(1):153-64. https://doi.org/10. 9756/iajse/v11i1/iajse1118.
7. Ahmad Zaki NA, Mahmud S, Fairuz Omar A. Ultraviolet Protection Properties of Commercial Sunscreens and Sunscreens Containing Zno Nanorods. J Phys Conf Ser. 2018; 1083(1): 12012. . https://doi.org/10.1088/1742-6596/1083/1/012012.
8. Wenyue Z, Rajesh Ramanathan SU. Sunscreen testing: A critical perspective and future roadmap. TrAC Trends Anal Chem. 2022; 157: 116724. https://doi.org/10.1016/j.trac.2022.116724.
9. Rigano L, Mezzanotte A, Lohman M, Kujansivu L. Hydrogenated polydecanes and high SPF physical sunscreens. Cosmetics & Toiletries. 2015; 79-85.
10. Wright PFA. Realistic exposure study assists risk assessments of ZnO nanoparticle sunscreens and allays safety concerns. J Invest Dermatol. 2019; 139(2): 277–8. https://doi.org/10.1016/j.jid. 2018.09. 014.
11. Reinosa JJ, Docio CMÁ, Ramírez VZ, Lozano JFF. Hierarchical nano ZnO-micro TiO2 composites: High UV protection yield lowering photodegradation in sunscreens. Ceram Int. 2018; 44(3): 2827-34. https://doi.org/10.1016/j.jid.2018.09.014.
12. Ilić K, Selmani A, Milić M, Glavan TM, Zapletal E, Ćurlin M, et al. The shape of titanium dioxide nanomaterials modulates their protection efficacy against ultraviolet light in human skin cells. J Nanoparticle Res. 2020; 22(3): 1-13. https://doi.org/

10.1007/s11051-020-04791-0.
13. Lin CH, Lin MH, Chung YK, Alalaiwe A, Hung CF, Fang JY. Exploring the potential of the nano-based sunscreens and antioxidants for preventing and treating skin photoaging. Chemosphere. 2024; 347: 140702. https://doi.org/10.1016/j.chemosphere.2023. 140702.
14. Bernstein EF, Sarkas HW, Boland P. Iron oxides in novel skin care formulations attenuate blue light for enhanced protection against skin damage. J Cosmet Dermatol. 2021;20(2):532-537. https://doi.org/10. 1111/jocd.13803.
15. Schneider SL, Lim HW. A review of inorganic UV filters zinc oxide and titanium dioxide. Photodermatol Photoimmunol Photomed. 2019;35(6):442–6. https:// doi.org/10.1111/phpp.12439.
16. Jafari H, Khajeh Mehrizi M, Fattahi S. The effect of inorganic nanoparticles on camouflage properties of cotton/polyester fabrics. Prog Color Colorant Coat. 2016;9(1):29-40. https://doi.org/10.30509/ pccc.2016. 75872.
17. Le Thi Nhu Ngoc VVTO, Ju-Young M, Minhe C, Duckshin YCL. Recent trends of sunscreen cosmetic: an update review, Cosmetics, 2019;6(4):64. https://doi.org/10.3390/COSMETICS6040064.
18. Sagadevan S, Imteyaz S, Murugan B, Anita Lett J, Sridewi N, Weldegebrieal GK, et al. A comprehensive review on green synthesis of titanium dioxide nanoparticles and their diverse biomedical applications. Green Process Synth. 2022; 11(1):44–63. https://doi.org/10.3390/COSMETICS6040064.
19. Wang J, Wang Z, Wang W, Wang Y, Hu X, Liu J, et al. Synthesis, modification and application of titanium dioxide nanoparticles: a review. Nanoscale. 2022; 6709-34. https://doi.org/10.1039/d1nr08349j.
20. Smijs TG, Pavel S. Titanium dioxide and zinc oxide nanoparticles in sunscreens: Focus on their safety and effectiveness. Nanotechnol Sci Appl. 2011; 4(1): 95-112. https://doi.org/10.2147/nsa.s19419.
21. Haratian Nezhad E, Haratizadeh H, Mohammad Kari B. Influence of thickness and number of silver layers in the electrical and optical properties of ZnO/Ag/ZnO/Ag/ZnO ultra-thin films deposited on the glass for low-emissivity applications. Prog Color Colorant Coat. 2019;12(2):83-91. https://doi.org/10. 30509/pccc.2019.81543.
22. Asadi F, Jannesari A, Arabi AM. Synthesis and characterization of well-dispersed zinc oxide quantum dots in epoxy resin using epoxy siloxane surface modifier. Prog Color Colorant Coat. 2023; 16(4): 399-408. https://doi.org/10.30509/pccc.2023.167118.1210.
23. Díaz-Reyes J, Martínez-Juárez J, Galeazzi R, Juárez-Díaz G, Galván-Arellano M, Rodríguez-Fragoso P, E. Lopez-Cruz. Structural and optical characterization of ZnO layers grown by chemical bath deposition activated by means microwaves. In: Frazao O, editor. Proceedings of the 3rd WSEAS international conference on Advances in sensors, signals and materials; 2010 Nov 3-5; Faro, Portugal. Stevens Point, Wiscons, United States: World Scientific and Engineering Academy and Society (WSEAS) 2010. p. 105-109.
24. Vaudagna MV, Aiassa V, Marcotti A, Pince Beti MF, Constantín MF, Pérez MF, et al. Titanium Dioxide Nanoparticles in sunscreens and skin photo-damage. Development, synthesis and characterization of a novel biocompatible alternative based on their in vitro and in vivo study. J Photochem Photobiol. 2023; 15: 100173. https://doi.org/10.1016/j.jpap.2023.100173.
25. Wang X. The comparison of titanium dioxide and zinc oxide used in sunscreen based on their enhanced absorption. Appl Comput Eng. 2023; 24(1): 237-45. https://doi.org/10.54254/2755-2721/24/20230715.
26. Ruocco V, Morganti P, Wolf D WR. Sunscreens. Clin Dermatol. 2001;19(4):452-459. https://doi.org/10. 1016/s0738-081x(01)00190-0.
27. Ann LC, Mahmud S, Seeni A, Bakhori SKM, Sirelkhatim A, Mohamad D, Hasan H. Structural morphology and in vitro toxicity studies of nano- and micro-sized zinc oxide structures. J Environ Chem Eng. 2015;3(1):436-44. https://doi.org/10.1016/j. jece. 2014.12.015.
28. Agarwal S, Jangir LK, Rathore KS, Kumar M, Awasthi K. Morphology-dependent structural and optical properties of ZnO nanostructures. Appl Phys A. 2019;125(8):553. https://doi.org/10.1016/j.jece. 2014. 12.015.
29. Davis K, Yarbrough R, Froeschle M, White J, Rathnayake H. Band gap engineered zinc oxide nanostructures: Via a sol-gel synthesis of solvent driven shape-controlled crystal growth. RSC Adv. 2019;9(26):14638-48. https://doi.org/10.1039/c9ra 02091h.
30. Mishra SK, Srivastava RK, Prakash SG. ZnO nano-particles: Structural, optical and photoconductivity characteristics. J Alloys Compoun. 2012;539:1-6. https://doi.org/10.1016/j.jallcom.2012.06. 024.
31. Hull MS, Bowman DM, Nanotechnology environmental health and safety. risks, regulation, and management, 3rd ed., Elsevier B.V, 2019. https://doi. org/10.1016/C2016-0-04525-4.
32. Butler H. Poucher's Perfumes, Cosmetics and Soaps. 10th ed. Butler H, editor. London: Kluwer Academic Publishers; 2000. 628–635. https://doi.org/10.1007/ 978-94-017-2734-1
33. Pinnell SR, Fairhurst D, Gillies R, Mitchnick MA, Kollias N. Microfine zinc oxide is a superior sunscreen ingredient to microfine titanium dioxide. Dermatol Surg. 2000; 26: 309-14. https://doi.org/10. 1046/j.1524-4725.2000.99237.x.
34. Afshar FTP, Ramezanian N, Behzadpour M. Identification and evaluation of replaced materials of titanium dioxide pigment in alkyd resins and investigation of their properties. Prog Color Colorant Coat. 2020; 13(3):167-75. https://doi.org/10.30509/ pccc. 2020.81627.
35. Caswell M. Sunscreen formulation and testing. Allured's Cosmetics & Toiletries. 2001 Sep;116(9):49-

60. https://doi.org/0361-4387/01/0009-0049$05.00/ 0.
36. Goh EG, Xu X, McCormick PG. Effect of particle size on the UV absorbance of zinc oxide nano-particles. Scr Mater. 2014;78-79:49-52. https://doi.org/10.1016/j.scriptamat.2014.01.033.
37. Özgür Ü, Alivov YI, Liu C, Teke A, Reshchikov MA, Doğan S, et al. A comprehensive review of ZnO materials and devices. J Appl Phys. 2005; 98(4): 1-https://doi.org/103. 10.1063/1.1992666.
38. Antony Lilly Grace M, Veerabhadra Rao K, Anuradha K, Judith Jayarani A, Arun kumar A, Rathika A. X-ray analysis and size-strain plot of zinc oxide nanoparticles by Williamson-Hall. Mater Today Proc. 2023;92:1334–9; https://doi.org/10.1016/j. matpr. 2023.05.492.
39. Mohan AC, Renjanadevi B. Preparation of Zinc Oxide Nanoparticles and its Characterization Using Scanning Electron Microscopy (SEM) and X-Ray Diffraction(XRD). Procedia Technol. 2016; 24: 761–766. https://doi.org/10.1016/j.protcy.2016.05.078.
40. Bulcha B, Leta Tesfaye J, Anatol D, Shanmugam R, Dwarampudi LP, Nagaprasad N, et al. Synthesis of Zinc Oxide Nanoparticles by Hydrothermal Methods and Spectroscopic Investigation of Ultraviolet Radiation Protective Properties. J Nanomater. 2021 Jan 1;2021(1):8617290. https://doi.org/10. 1155/2021/ 8617290.
41. Bajpai G, Moirangthem I, Sarkar S, Barman SR, Vinod CP, Bajpai S, et al. Role of Li^{+} and Fe^{3+} in modified ZnO: Structural, vibrational, opto-electronic, mechanical and magnetic properties. Ceram Int. 2019;45(6):7232-43. https://doi.org/10.1016/j. ceramint. 2019. 01.004.
42. Maru AD, Lahoti SR. Formulation and evaluation of moisturizing cream containing sunflower wax, Nternational J Pharm Pharm Sci. 2018; 10(11): 54-59 https://doi.org/10.22159/ijpps.2018v10i11.28645.
43. Eros I, Kónya IM, Csóka M. Study of the structure of coherent emulsions. Int J Pharm. 2003; 256: 75-84. https://doi.org/10.1016/S0378-5173(03)00064-4.
44. Gaska K, Xu X, Gubanski RK. Electrical, mechanical, and thermal properties of LDPE graphene nanoplatelets composites produced by means of melt extrusion process. Polymers (Basel). 2017; 9(11). https://doi.org/10.3390/polym9010011.
45. Maryanti. EETES. Determination Of SPF (Sun Protection Factor) Values And Evaluation Of Sunscreen Cream With ZnO and TiO_2 Nanoparticles Combination In Vitro As Active Ingredients. 2019. https://doi.org/10.1590/S1516-93322004000300014.
46. Dutra EA, Da Costa E Oliveira DAG, Kedor-Hackmann ERM, Miritello Santoro MIR. Determination of sun protection factor (SPF) of sunscreens by ultraviolet spectrophotometry. Rev Bras Ciencias Farm J Pharm Sci. 2004; 40(3): 381-5. https://doi.org/10.1590/S1516-93322004000300014.

How to cite this article:
Gozalabad Ghorbani M, Ghazitabar A, Gholami F, Naderi M, Fatmehsari Haghshenas D. Investigating the Effect of Zinc Oxide Nanoparticles on the Absorption of Ultraviolet Radiation for Enhancing the Efficacy of Sunscreen Products. Prog Color Colorants Coat. 2026;19(1):47-65. https://doi.org/10.30509/pccc.2025.167471.1365.